



Application of the unified gas-kinetic scheme to ES-BGK models for the simulation of rarefied gas flows encountered in atmospheric re-entry

Céline Baranger¹, Alexis Coëpeau², Luc Mieussens³

Abstract

The Unified Gas-Kinetic Scheme (UGKS) differs from traditional deterministic methods in gas dynamics by providing a unified approach capable of resolving flow regimes, from rarefied to continuum, with a simulation time that remains independent of the flow regime. Its effectiveness in handling complex and multi-scale flows has been mainly demonstrated through Shakhov or Rykov models. Additionally, it has been applied to ES-BGK type models, although its use has thus far been restricted to monoatomic effects only.

Here, we aim to explore the application of UGKS to ES-BGK models in greater depth, extending its use from monoatomic to polyatomic gases by employing recent formulations. Particular attention will be given to validating this adaptation through numerical comparisons with codes from the literature, such as SPARTA for non-vibrating gas flows and PIClas for other cases, as it can handle polyatomic ES-BGK models, including vibrational phenomena.

Keywords: Ellipsoidal Statistical BGK models, Unified Gas-Kinetic Scheme, gas dynamics

1. Introduction

During re-entry of space shuttle, various kind of atmospheric layers are encountered at high speed. To develop such shuttles, one has to compute parietal flux and aerodynamic coefficients on these objects, which implies to simulate precisely air flows around them. In the upper layers of the atmosphere, the air is in a rarefied state, the mean free path of the particles of air is not so small as compared to the size of the shuttle. In such a rarefied regime, the Knudsen number which is the ratio between the mean free path λ and a characteristic length L ($Kn = \frac{\lambda}{L}$) is larger than 0.01, and is used to discriminate rarefied regime from continuous regime (at low altitude) and also from the molecular regime (very high altitude). In the continuous regime, the flow is described by the compressible Navier-Stokes equations of Gas Dynamics. In the molecular regime, the Newton law is used to describe quantities at the boundary of the shuttle. In the rarefied regime, the Navier-Stokes equations are no longer valid and the use of the kinetic theory of gas via the Boltzmann equation is needed. The evolution of the molecules of the gas is then described by a mass density distribution in phase space, which is a solution of the Boltzmann equation.

One of the earliest simplified models of the Boltzmann equation is the Bhatnagar-Gross-Krook (BGK) model [3, 21]. It was developed to enable faster numerical simulations of transport phenomena within a monoatomic gas in a transitional state between rarefied and continuous regimes.

However, the BGK model has the disadvantage of only being able to simulate gas flows with a unitary Prandtl number. Thus, it cannot accurately predict the propagation of thermal effects relative to dynamic effects. To address this limitation, more advanced models such as the Ellipsoidal-Statistical BGK (ES-BGK) model [10] and the Shakhov-BGK model [20] were introduced. These models are capable of correctly recovering a Prandtl number of 2/3 for monoatomic gases, thereby providing a more accurate

¹CEA-CESTA, 15 Av. des Sablières, 33114 Le Barp, France, celine.baranger@cea.fr

²CEA-CESTA, 15 Av. des Sablières, 33114 Le Barp, France, alexis.coepeau@cea.fr

³Univ. Bordeaux, CNRS, Bordeaux INP, IMB, UMR 5251, F-33400, Talence, France, luc.mieussens@math.u-bordeaux.fr

representation of thermal dynamics and a more realistic continuous asymptotic limit representation. Unlike the Shakhov model, the monoatomic ES-BGK model ensures the positivity of the mass distribution, and satisfies the H-theorem [1]. Consequently, it retains the same fundamental properties as the original BGK model and the Boltzmann equation. This model has subsequently been extended to diatomic gases [1] and has undergone various modifications, such as capturing rotational and vibration energy relaxation processes [8, 13, 17].

For a long time, these kinetic models were only solved numerically using methods that introduce excessive numerical diffusion, which was much higher than the physical diffusion processes described by these models in their Navier-Stokes asymptotic limit. To address this, a common approach was to use meshes sized according to the mean free path of particles in the flow. However, this led to extremely time-consuming methods as the density of the resolved flow increased. Since 2010, K. Xu et al. have been developing a unified method known as the "Unified Gas-Kinetic Scheme" (UGKS) [22]. This singular method allows for the accurate resolution of all ranges of flows with a computational cost independent of the rarefaction of the gas, as its numerical diffusion is controlled [7]. In particular, this scheme can reduce itself to either a Navier-Stokes or a free-stream resolving scheme, depending on the asymptotic regime simulated.

The UGKS has only been applied to monoatomic ES-BGK models [6, 11]. Here, we propose to extend it to phenomena typical of diatomic models, such as rotational and vibration energy storages, as described by [1, 8, 13, 17]. The outline of the paper is as follows. Section 2 is dedicated to the definition of the ellipsoidal statistical BGK class of model. Section 3 presents and adapts the unified gas kinetic scheme to ES-BGK models. The results of numerical simulations conducted on several test cases are provided in Section 4. Finally, Section 5 presents the conclusions of this paper.

2. The model

2.1. Mass distribution and relationship with macroscopic quantities

To describe the dynamics of a polyatomic gas, a microscopic distribution of mass F is used. It is defined over the phase space $(t, \boldsymbol{x}, \boldsymbol{v}, \epsilon, \mathbf{i}) \in \mathbb{R}^+ \times \mathbb{R}^{D_{\boldsymbol{x}}} \times \mathbb{R}^{D_{\boldsymbol{v}}} \times \mathbb{R}^+ \times \mathbb{N}$ such that, at any time $t \in \mathbb{R}^+$, $F(t, \boldsymbol{x}, \boldsymbol{v}, \epsilon, \mathbf{i}) d\boldsymbol{x} d\boldsymbol{v} d\epsilon$ represents the mass excited at the ith level of discrete vibrational energy, in the volume $d\boldsymbol{x} d\boldsymbol{v} d\epsilon$ centered at the spatial point \boldsymbol{x} , the particle velocity \boldsymbol{v} and the rotational energy ϵ . Formally, $D_{\boldsymbol{x}}$ and $D_{\boldsymbol{v}}$ represent the number of spatial and kinetic dimensions, respectively, and δ will denote the number of continuous rotational degrees of freedom.

In practice, D_x and D_v are typically set to 3, as particles can exist and move in three-dimensional space, and δ is set to 2 for diatomic molecules. For such molecules, the harmonic oscillator model is commonly used to determine the vibration energy distribution, relying on a gas-characteristic vibration temperature T_0 . In this model, the vibration energy of the ith excitation level is iR_sT_0 , where R_s is the constant of the gas. In more general cases ($\delta > 2$), the vibration energy could be modeled by a summation over multiple harmonic oscillators corresponding to multiple vibration modes. For the purposes of this paper, only diatomic molecules are considered.

The mass density, momentum, and total energy, which are macroscopic quantities depending on space and time only, are recovered as velocity and internal energy moments of the microscopic distribution F:

$$\rho = \langle F \rangle_{\boldsymbol{v},\epsilon,i},\tag{1}$$

$$\rho \boldsymbol{u} = \langle \boldsymbol{v} F \rangle_{\boldsymbol{v}, \epsilon, i}, \tag{2}$$

$$E = E_c + E_{tr} + E_{rot} + E_{vib},\tag{3}$$

where the modal energies are defined as:

$$E_c = \frac{1}{2}\rho |\boldsymbol{u}|^2, \qquad E_{tr} = \langle \frac{1}{2}|\boldsymbol{v} - \boldsymbol{u}|^2 F \rangle_{\boldsymbol{v}, \epsilon, i}, \qquad (4)$$

$$E_{rot} = \langle \epsilon F \rangle_{\boldsymbol{v},\epsilon,i}, \qquad E_{vib} = \langle iR_s T_0 F \rangle_{\boldsymbol{v},\epsilon,i},$$
 (5)

with $\langle \chi \rangle_{\boldsymbol{v},\epsilon,i} = \sum_{i=0}^{+\infty} \int_{\mathbb{R}^{+}} \int_{\mathbb{R}^{D\boldsymbol{v}}} \chi d\boldsymbol{v} d\epsilon$ for any distribution $\chi(\boldsymbol{v},\epsilon,i)$. Moreover, additional quantities, such as the temperatures associated with the different energy modes, can be derived as follows:

$$E_{tr} = \frac{D_{v}}{2} \rho R_{s} T_{tr}, \quad E_{rot} = \frac{\delta}{2} \rho R_{s} T_{rot}, \quad E_{vib} = \rho \frac{R_{s} T_{0}}{\exp(T_{0}/T_{vib}) - 1}.$$
 (6)

In these expressions, the subscripts tr, rot and vib refer to the translational, the rotational and the vibrational modes of energy. The equilibrium temperature T_{eq} is associated with all these internal modes:

$$E_{tr} + E_{rot} + E_{vib} = \frac{D_{v}}{2} \rho R_{s} T_{eq} + \frac{\delta}{2} \rho R_{s} T_{eq} + \rho \frac{R_{s} T_{0}}{\exp(T_{0}/T_{eq}) - 1}.$$
 (7)

Finally, for further needs, we introduce the following invertible energy functions with respect to any positive temperature T:

$$e_{tr}(T) = \frac{D_{v}}{2}R_{s}T, \quad e_{rot}(T) = \frac{\delta}{2}R_{s}T, \quad e_{vib}(T) = \frac{R_{s}T_{0}}{\exp(T_{0}/T) - 1}.$$
 (8)

2.2. The Ellipsoidal-Statistical BGK models for diatomic gases

The distribution F is governed by a Boltzmann type of equation for dilute polyatomic gas in the absence of any external force field:

$$(\partial_t F + \mathbf{v} \cdot \nabla_{\mathbf{x}} F)(t, \mathbf{x}, \mathbf{v}, \epsilon, i) = Q(F)(t, \mathbf{x}, \mathbf{v}, \epsilon, i). \tag{9}$$

The right-hand term of this equation is the *collision operator*, which is the term modeled to facilitate and accelerate simulations of rarefied flows. In the ES-BGK models framework [1, 8, 10, 13, 17] is it proposed to model the collision operator as a relaxation toward a local anisotropic equilibrium:

$$Q(F)(t, \boldsymbol{x}, \boldsymbol{v}, \epsilon, i) = \frac{1}{\tau} (G[F] - F)(t, \boldsymbol{x}, \boldsymbol{v}, \epsilon, i),$$
(10)

where $G[F](\cdot, \cdot, \boldsymbol{v}, \epsilon, i)$ is a combination of multiple pseudo-equilibrium distributions, each corresponding to a specific energy mode. In the most general case, accounting for translational, rotational, and vibrational degrees of freedom of particles, the near-equilibrium state G[F] is expressed as the product of G_{tr} , G_{rot} , and G_{vib} defined as follows:

$$G_{tr}(\boldsymbol{v}) = \frac{\rho}{\sqrt{|2\pi\mathcal{T}|}} \exp\left(-\frac{1}{2}(\boldsymbol{v} - \boldsymbol{u})\mathcal{T}^{-1}(\boldsymbol{v} - \boldsymbol{u})\right), \tag{11}$$

$$G_{rot}(\epsilon) = \frac{\Lambda_{\delta}}{(R_{s}T_{rot}^{rel})^{\delta/2}} \epsilon^{\frac{\delta-2}{2}} \exp\left(-\frac{\epsilon}{R_{s}T_{rot}^{rel}}\right),\tag{12}$$

$$G_{vib}(\mathbf{i}) = (1 - \exp(-T_0/T_{vib}^{rel})) \exp\left(-\mathbf{i}\frac{T_0}{T_{vib}^{rel}}\right). \tag{13}$$

Here, the constant Λ_{δ} is defined in terms of the standard gamma function as $\Lambda_{\delta} = 1/\Gamma(\delta/2)$. The terms T_{rot}^{rel} and T_{vib}^{rel} represent the rotational and vibrational relaxation temperatures, respectively, while \mathcal{T}/R_s denotes a relaxation temperature tensor. These three last quantities describe the exchange of energy between translational, rotational and vibrational modes. The tensor \mathcal{T}/R_s is related to the anisotropic tensor of temperature Θ/R_s , the Prandtl number Pr, and the relaxation translational temperature T_{tr}^{rel} as follows:

$$\mathcal{T} = R_s T_{tr}^{rel} I_{D_v} + \left(1 - \frac{1}{\Pr}\right) \left[\Theta - R_s T_{tr} I_{D_v}\right],\tag{14}$$

$$\Theta = \frac{1}{\rho} \langle (\boldsymbol{v} - \boldsymbol{u}) \otimes (\boldsymbol{v} - \boldsymbol{u}) F \rangle_{\boldsymbol{v}, \epsilon, i}, \tag{15}$$

$$T_{tr}^{rel} = e_{tr}^{-1}(e_{tr}^{rel}), \quad T_{rot}^{rel} = e_{rot}^{-1}(e_{rot}^{rel}), \quad T_{vib}^{rel} = e_{vib}^{-1}(e_{vib}^{rel}). \tag{16}$$

While the previous expressions are common to all ES-BGK models, relaxation modal energies e_{tr}^{rel} , e_{rot}^{rel} and e_{vib}^{rel} need to be defined. In fact, they differ from one ES-BGK model to another depending on the energetic relaxation process modeled.

In the Holway [10], the rotational and vibrational modes of molecules are not considered, and the translational relaxation energy is:

$$e_{tr}^{rel} = e_{tr}(T_{tr}). (17)$$

In the Andriès model [1], the vibrational mode of molecules is not modeled and the relaxation energies are:

$$e_{tr}^{rel} = e_{tr}(T_{tr}) + \frac{1}{Z_{rot}}(e_{tr}(T_{eq}) - e_{tr}(T_{tr})), \tag{18}$$

$$e_{rot}^{rel} = e_{rot}(T_{rot}) + \frac{1}{Z_{rot}}(e_{rot}(T_{eq}) - e_{rot}(T_{rot})).$$
(19)

Finally, in the Pfeiffer model [13, 17], which include both rotational and vibrational energies, the relaxation energies are:

$$e_{tr}^{rel} = e_{tr}(T_{tr}) - \frac{\tau}{Z_{rot}\tau_C}(e_{rot}(T_{tr}) - e_{rot}(T_{rot})) - \frac{\tau}{Z_{vib}\tau_C}(e_{vib}(T_{tr}) - e_{vib}(T_{vib})), \tag{20}$$

$$e_{rot}^{rel} = e_{rot}(T_{rot}) + \frac{\tau}{Z_{rot}\tau_C}(e_{rot}(T_{tr}) - e_{rot}(T_{rot})), \tag{21}$$

$$e_{vib}^{rel} = e_{vib}(T_{vib}) + \frac{\tau}{Z_{vib}\tau_C}(e_{vib}(T_{tr}) - e_{vib}(T_{vib})).$$
 (22)

In the above definitions, τ_C is the average collision time of molecules, and Z_{rot} or Z_{vib} are the average numbers of collisions required to involve energy exchange with the rotational mode or the vibrational mode, respectively. These are common parameters in Direct Simulation Monte Carlo (DSMC) methods and typically range from 3 to 20 and from 50 to 100'000, respectively. These values can either be treated as constants or expressed as functions of the translational temperature, as described in [12, 15, 16].

Furthermore, the relaxation time τ of the model is related to the fluid viscosity and the pressure as follows:

$$\tau = \frac{\mu}{\Pr p}, \qquad p = \rho R_s T_{tr}. \tag{23}$$

Finally, all these models have been proven [1, 8, 13], under reasonable conditions, to be well defined, conserve mass, momentum, and total energy, and admit the "Maxwellian state" M below as full equilibrium:

$$M[F](\mathbf{v}, \epsilon, \mathbf{i}) = M_{tr}(\mathbf{v}) M_{rot}(\epsilon) M_{vib}(\mathbf{i}) , \qquad (24)$$

$$M_{tr}(\mathbf{v}) = \frac{\rho}{(2\pi R_s T_{eq})^{D_{\mathbf{v}}/2}} \exp\left(-\frac{|\mathbf{v} - \mathbf{u}|^2}{2R_s T_{eq}}\right),\tag{25}$$

$$M_{rot}(\epsilon) = \frac{\Lambda_{\delta}}{(R_s T_{eq})^{\delta/2}} \epsilon^{\frac{\delta-2}{2}} \exp\left(-\frac{\epsilon}{R_s T_{eq}}\right), \tag{26}$$

$$M_{vib}(i) = (1 - \exp(-T_0/T_{eq})) \exp\left(-i\frac{T_0}{T_{eq}}\right).$$
 (27)

They also yield correct transport coefficients and Prandtl number in the hydrodynamic limit, and satisfy the H-theorem.

3. The UGKS

The numerical method will be presented in a 1D spatial framework for simplicity, although it can be extended to 2D or 3D. We begin by outlining the framework before constructing the UGKS for ES-BGK models.

3.1. A Discrete-Velocity-Model - Finite-Volume framework

The ES-BGK model is an integro-differential equation expressed in an advection-relaxation form, which makes the finite volume framework intrinsically well suited. In this context, all phases of the equation will be discretized. In that sense, the time space \mathbb{R}^+ and the physical space \mathbb{R} are divided into intervals $([t^n,t^{n+1}])_{n\in\mathbb{N}}$ and $([x_{i-\frac{1}{2}},x_{i+\frac{1}{2}}])_{i\in\mathbb{Z}}$, respectively. For simplicity, the spatial interval length will be constant, denoted as $x=x_{i+\frac{1}{2}}-x_{i-\frac{1}{2}}$. Finally, following the methodology of Discrete Velocity Models (DVM), we consider a finite velocity set $\mathcal{V}\subset\mathbb{R}^3$ and the projection of the model equation (9-10) on this set.

In association with the velocity set \mathcal{V} , we choose a quadrature rule on the velocity phase that enables the computation of the moments of the microscopic distributions set. In the following, $\langle \chi \rangle_{\mathcal{V}}$ will denote the velocity quadrature rule integration of a distribution $\chi(\boldsymbol{v})$, while $\langle X \rangle_{\mathcal{V},\epsilon,i}$ will refer to the combination of this velocity quadrature rule integration, continuous integration over the phase ϵ , and summation over the phase i of a distribution $X(\boldsymbol{v},\epsilon,i)$.

We introduce the distribution families $(F_{i,k}^n(\cdot,\cdot))_{n\in\mathbb{N},i\in\mathbb{Z},k\leqslant|\mathcal{V}|}$ and $(G_{i,k}^n(\cdot,\cdot))_{n\in\mathbb{N},i\in\mathbb{Z},k\leqslant|\mathcal{V}|}$ defined as the mean value of F and G on a spatial cell $[x_{i-\frac{1}{2}},x_{i+\frac{1}{2}}]$ at time t^n , and velocity \boldsymbol{v}_k :

$$\begin{pmatrix} F \\ G \end{pmatrix}_{i,k}^{n} (\epsilon, \mathbf{i}) = \frac{1}{\Delta x} \int_{x_{i-\frac{1}{2}}}^{x_{i+\frac{1}{2}}} \begin{pmatrix} F \\ G \end{pmatrix} (t^n, x, \boldsymbol{v}_k, \epsilon, \mathbf{i}) dx. \tag{28}$$

Integrating (9-10) at velocity v_k over the spatial volume $[x_{i-\frac{1}{2}},x_{i+\frac{1}{2}}]$ for the time interval $[t^n,t^{n+1}]$ leads to the classical finite volume formulation:

$$F_{i,k}^{n+1}(\epsilon, \mathbf{i}) = F_{i,k}^{n}(\epsilon, \mathbf{i}) - \frac{\Delta t}{\Delta x} \left[\phi_{i+\frac{1}{2},k}^{n} - \phi_{i-\frac{1}{2},k}^{n} \right] (\epsilon, \mathbf{i}) + \int_{t^{n}}^{t^{n+1}} \int_{x_{i-\frac{1}{k}}}^{x_{i+\frac{1}{2}}} \frac{G - F}{\tau} (t, x, \boldsymbol{v}_{k}, \epsilon, \mathbf{i}) dx dt, \tag{29}$$

$$\phi_{i+\frac{1}{2},k}^{n}(\epsilon,\mathbf{i}) = \frac{1}{\Delta t} \int_{t^{n}}^{t^{n+1}} \mathbf{v}_{k} F(t, x_{i+\frac{1}{2}}, \mathbf{v}_{k}, \epsilon, \mathbf{i}) dt.$$

$$(30)$$

Finally, for further needs, we also introduce the discrete moments $(\boldsymbol{W}_{i}^{n})_{n\in\mathbb{N},i\in\mathbb{Z}}$ of $(F_{i,k}^{n}(\cdot,\cdot))_{n\in\mathbb{N},i\in\mathbb{Z},k\leqslant|\mathcal{V}|}$ with respect to the operator $\langle\cdot\rangle_{\mathcal{V},\epsilon,i}$:

$$\boldsymbol{W}_{i}^{n} = \left\langle \boldsymbol{m}_{k}(\epsilon, i) F_{i,k}^{n}(\epsilon, i) \right\rangle_{\mathcal{V}_{\epsilon, i}}, \tag{31}$$

$$\boldsymbol{m}_k(\epsilon, i) = \begin{pmatrix} 1 & \boldsymbol{v}_k & \boldsymbol{v}_k \otimes \boldsymbol{v}_k & \epsilon & iR_sT_0 \end{pmatrix}^T.$$
 (32)

Integrating (29-30) with $\langle \cdot \rangle_{\mathcal{V},\epsilon,i}$ naturally leads to a finite volume scheme on moments W.

The finite-volume formulation (29-30) is an exact expression. However, the relaxations and flux terms must be approximated. Generally, they are considered separately using a splitting method. The relaxation term is commonly approximated by a quadrature method in time (e.g., forward Euler, backward Euler, Crank-Nicolson), while the flux term is estimated either by a high-order reconstruction or by characteristic techniques, both applied to the collisionless transport equation.

3.2. A multi-scale formulation of the numerical flux

The key idea of the UGKS [22] is to use the entire model equation (9-10) to express the evolution of the distribution F during the time interval $[t^n, t]$ at cell interface position $(x_{i\pm\frac{1}{2}}, \mathbf{v}_k, \epsilon, \mathbf{i})$, which is required to compute the numerical fluxes (30). This approach differs from conventional methods by accounting not only for free transport but also for relaxation towards equilibrium during the distribution transport itself. Specifically, by using the characteristic method on the model equation (9-10), for a time-independent τ over the interval $[t^n, t]$ and for any $(\mathbf{x}, \mathbf{v}, \epsilon, \mathbf{i})$, we get:

$$F(t, \boldsymbol{x}, \boldsymbol{v}, \epsilon, i) = \exp\left(-\frac{t - t^n}{\tau}\right) F(t^n, \boldsymbol{x} - \boldsymbol{v}(t - t^n), \epsilon, i)$$

$$+ \int_{t^n}^t \exp\left(-\frac{t - s}{\tau}\right) \frac{1}{\tau} G(s, \boldsymbol{x} - \boldsymbol{v}(t - s), \boldsymbol{v}, \epsilon, i) ds.$$
(33)

The above equation, which represents the distribution F at $(t, \boldsymbol{x}, \boldsymbol{v}, \epsilon, i)$, is a balance between the collisionless transport of the initial distribution and the transport of the equilibrium distribution.

3.3. Second order reconstruction of both microscopic and macroscopic parts of the flux

An exact numerical flux based on equation (33) would require knowledge of the distributions F and G at any $(t, \boldsymbol{x}, \boldsymbol{v}, \epsilon, i) \in \mathbb{R}^+ \times \mathbb{R}^{D_{\boldsymbol{x}}} \times \mathbb{R}^{D_{\boldsymbol{v}}} \times \mathbb{R}^+ \times \mathbb{N}$. For practical computations, approximations must be made. To develop a second-order scheme, these distributions are approximated by linear constructions based on discretized distributions (28). A common assumption in the finite volume framework is to consider these mean values at the center of the spatial cells. In the UGKS framework [22], τ is considered constant near the interface, reconstructions \mathbb{F} for F are performed for each cell, while reconstructions \mathbb{G} for G are realized for each cell interface as formalized below:

$$\mathbb{F}_{i,k}^n(x,\epsilon,i) = F_{i,k}^n(\epsilon,i) + \delta_x F_{i,k}^n(\epsilon,i)(x-x_i), \tag{34}$$

$$\mathbb{G}_{i+\frac{1}{2},k}(t,x,\epsilon,i) = G_{i+\frac{1}{2},k}^{n}(\epsilon,i) + \delta_{x}G_{i+\frac{1}{2},k}^{n}(\epsilon,i)(x-x_{i+\frac{1}{2}}) + \delta_{t}G_{i+\frac{1}{2},k}^{n}(\epsilon,i)(t-t^{n}), \tag{35}$$

where F, $\delta_x F$, G, $\delta_x G$, and $\delta_t G$ should be discrete approximations of microscopic and equilibrium distributions, and their partial derivatives. For stability purposes, $\delta_x F$ is defined in each cell as a limited slope based on forward and backward slope and a TVD (Total Variation Diminishing) limiter [22]. The microscopic part of (33) is replaced by the appropriate linear approximation of the microscopic distribution, depending on the cell location of $x - v(t - t^n)$. Thus, following this point and for further needs, we define:

$$\delta_x F_{i+\frac{1}{2},k}^n(\epsilon, \mathbf{i}) = \begin{cases} \delta_x F_{i,k}^n(\epsilon, \mathbf{i}) & \text{if } v_{k,x} \geqslant 0, \\ \delta_x F_{i+1,k}^n(\epsilon, \mathbf{i}) & \text{if } v_{k,x} < 0. \end{cases}$$
(36)

For the macroscopic reconstruction (35), we first require $G_{i+\frac{1}{2},k}^n(\epsilon,\mathbf{i})$. This term is determined by the moments $\boldsymbol{W}_{i+\frac{1}{2}}^n$ of F at the cell interface $i+\frac{1}{2}$ and time t^n . Consequently, the linear reconstructions $\mathbb{F}_{i,k}^n$ and $\mathbb{F}_{i+1,k}^n$ are employed to approximate these distributions and moments:

$$F_{i+\frac{1}{2},k}^{n}(\epsilon, \mathbf{i}) = \begin{cases} \mathbb{F}_{i,k}^{n}(x_{i+\frac{1}{2}}, \epsilon, \mathbf{i}) & \text{if } v_{k,x} \geqslant 0, \\ \\ \mathbb{F}_{i+1,k}^{n}(x_{i+\frac{1}{2}}, \epsilon, \mathbf{i}) & \text{if } v_{k,x} < 0, \end{cases}$$
(37)

$$W_{i+\frac{1}{2}}^{n} = \left\langle \boldsymbol{m}_{k}(\epsilon, i) F_{i+\frac{1}{2}, k}^{n}(\epsilon, i) \right\rangle_{\mathcal{V}, \epsilon, i}.$$
(38)

Finally, $(\mathcal{T}, e^{rel}_{rot}, e^{rel}_{vib})^n_{i+\frac{1}{2}}$ are determined using $\boldsymbol{W}^n_{i+\frac{1}{2}}$, and the appropriate formulation of the relaxation energies and tensor (14, 17, 18) or (20), after which $G^n_{i+\frac{1}{2},k}(\epsilon,\mathbf{i})$ can be deduced.

3.4. A major replacement in the macroscopic part of the flux

The last terms in (35) to approximate are the derivative components of \mathbb{G} , denoted as $\delta_x G$ and $\delta_t G$. Expressing these discrete spatial and temporal derivatives is a major step in constructing the fluxes of UGKS. The key idea employed here to ensure the proper behavior of the scheme is to replace the pseudo-equilibrium derivatives $\delta_x G$ and $\delta_t G$ with those of the corresponding Maxwellian distribution: $\delta_x M$ and $\delta_t M$.

First, it is important to remark that the derivatives of continuous states G and M are close to and of the same order as τ , as these states are. This is a classical result from Chapman-Enskog analysis (see, e.g., [1]). As a result, during a large time step $\Delta t \gg \tau$, from a continuous point of view, the average time derivative of M is very close to the average time derivative G, with an error depending on $\tau \ll \Delta t$.

Second, the discrete time derivative contribution in the numerical fluxes is mainly important in the continuum regime. An approximation of $O(\tau)$ on the derivative of equilibrium would not break down the Navier-Stokes asymptotic since it is a convenient replacement in the Chapmann-Enskog expansion.

The last, complementary, and more profound reason is stability. In the continuum regime, the numerical fluxes use the time derivative to compute the viscous part associated with the Navier-Stokes asymptotic, and also to achieve a second-order time scheme by indirectly computing the equilibrium at time $t^n + \Delta t/2$. This computation can be compared to a forward Euler method based on the time derivative at time t^n . However, the characteristic relaxation time of the pseudo-equilibrium state G toward the Maxwellian M is proportional to τ . Thus, using this time derivative with a time step $\Delta t/2 \gg \tau$ to estimate the evolution of G is not appropriate. It could over-relax the equilibrium state G and may lead to negative values of the distribution, in the continuum regime.

All these reasons explain why it is common in the UGKS framework to replace the derivative of the equilibrium state by the derivative of the Maxwellian. For example, this approach was used for the ES-BGK monoatomic model in [6] and for the Shakhov model in [23].

3.5. Construction of the equilibrium derivative terms

Spatial derivatives of the Maxwellian distribution are computed on both sides of the interface [22]:

$$\delta_{x} M_{i+\frac{1}{2},k}^{n}(\epsilon, \mathbf{i}) = \begin{cases} \delta_{x}^{-} M_{i+\frac{1}{2},k}^{n}(\epsilon, \mathbf{i}) & \text{if } v_{kx} \geqslant 0, \\ \delta_{x}^{+} M_{i+\frac{1}{2},k}^{n}(\epsilon, \mathbf{i}) & \text{if } v_{kx} < 0, \end{cases}$$
(39)

where $\delta_x^- M$ and $\delta_x^+ M$ are defined as follows. Using an exponential form of the continuous equilibrium state $M = \epsilon^{(\delta-2)/2} \exp(\boldsymbol{\eta} \cdot \boldsymbol{\alpha})$ with $\boldsymbol{\eta} = (1, \boldsymbol{v}, \frac{1}{2} |\boldsymbol{v}|^2 + \epsilon + \mathrm{i} R_s T_0)^T$ and $\boldsymbol{\alpha}$ a vector of conservative-related quantities, it can be shown that the derivatives of the continuous equilibrium state M are inner products of a velocity-internal energy dependent vector and a macroscopic vector: $\partial M = \boldsymbol{\eta} \cdot \partial \boldsymbol{\alpha} M$. So, we are looking for discrete derivatives $\delta_x^\pm M$ in the form:

$$\delta_x^{\pm} M_{i+\frac{1}{5},k}^n(\epsilon, \mathbf{i}) = \eta_k(\epsilon, \mathbf{i}) \cdot \delta_x^{\pm} \alpha_{i+\frac{1}{5}}^n M_{i+\frac{1}{5},k}^n(\epsilon, \mathbf{i}). \tag{40}$$

Using a chain rule, we get $\partial \boldsymbol{\alpha} = \partial_{\boldsymbol{U}} \boldsymbol{\alpha} \ \partial \boldsymbol{U}$, where $\boldsymbol{U} = (\rho, \rho \boldsymbol{u}, E)^T$ are the usual moments related to Maxwellian state (24) and $\partial_{\boldsymbol{U}} \boldsymbol{\alpha}$ is a Jacobian matrix that can be derived analytically. The vector \boldsymbol{U} can be deduced from \boldsymbol{W} and is both used to compute $M_{i+\frac{1}{3},k}^n$ using (24) and $\delta_x^{\pm} \boldsymbol{\alpha}$ as:

$$\delta_x^- \boldsymbol{\alpha}_{i+\frac{1}{2}}^n = \left[\partial_{\boldsymbol{U}} \boldsymbol{\alpha} \right]_{i+\frac{1}{2}}^n \frac{\boldsymbol{U}_{i+\frac{1}{2}}^n - \boldsymbol{U}_i^n}{\Delta x/2}, \tag{41}$$

$$\delta_x^+ \alpha_{i+\frac{1}{2}}^n = \left[\partial_U \alpha \right]_{i+\frac{1}{2}}^n \frac{U_{i+1}^n - U_{i+\frac{1}{2}}^n}{\Delta x/2}.$$
 (42)

For the time derivative, the same technique is applied. However, we first have to construct a discrete temporal macroscopic derivative $\delta_t U$, which is the discrete equivalent of $\partial_t U = \partial_t \langle \boldsymbol{\eta} F \rangle_{\boldsymbol{v},\epsilon,i} = \langle \boldsymbol{\eta} \ (\boldsymbol{v} \cdot \nabla_{\boldsymbol{x}} F) \rangle_{\boldsymbol{v},\epsilon,i}$. Following this, we set at the discrete level:

$$\delta_t \boldsymbol{U}_{i+\frac{1}{2}}^n = -\left\langle \boldsymbol{\eta}_k(\epsilon, i) v_{kx} \delta_x F_{i+\frac{1}{2}, k}^n(\epsilon, i) \right\rangle_{\mathcal{Y}_{\epsilon, i}}, \tag{43}$$

$$\delta_t \boldsymbol{\alpha}_{i+\frac{1}{2}}^n(\epsilon, \mathbf{i}) = \left[\partial_{\boldsymbol{U}} \boldsymbol{\alpha}\right]_{i+\frac{1}{2}}^n \delta_t \boldsymbol{U}_{i+\frac{1}{2}}^n, \tag{44}$$

$$\delta_t M_{i+\frac{1}{2},k}^n(\epsilon,i) = \eta_k(\epsilon,i) \cdot \delta_t \alpha_{i+\frac{1}{2}}^n M_{i+\frac{1}{2},k}^n(\epsilon,i).$$
(45)

3.6. Conclusion on the flux part of the scheme

Injecting the reconstructions in the numerical flux definition (30) leads to the following expression of the numerical flux ϕ :

$$\phi_{i+\frac{1}{3},k}^{n}(\epsilon,i) = v_{kx} \left[q_{1}G + q_{2}v_{kx}\delta_{x}M + q_{3}\delta_{t}M + q_{4}F + q_{5}v_{kx}\delta_{x}F \right]_{i+\frac{1}{3},k}^{n}(\epsilon,i).$$
(46)

The coefficients $(q_p)_{1\leqslant p\leqslant 5}$ are defined at the cell interface $i+\frac{1}{2}$ and at time t^n . They determine the scheme behavior depending on the local gas rarefaction $(\tau^n_{i+\frac{1}{2}})$ and the numerical resolution $(\Delta t/\tau^n_{i+\frac{1}{2}})$:

1.
$$q_1 = 1 - \frac{\tau}{\Delta t} (1 - e^{-\Delta t/\tau}),$$

2.
$$q_2 = 2\frac{\tau^2}{\Delta t}(1 - e^{-\Delta t/\tau}) - \tau(1 + e^{-\Delta t/\tau}),$$

3.
$$q_3 = \frac{\Delta t}{2} - \tau + \frac{\tau^2}{\Delta t} (1 - e^{-\Delta t/\tau}),$$

4.
$$q_4 = \frac{\tau}{\Delta t} (1 - e^{-\Delta t/\tau}),$$

5.
$$q_5 = \tau e^{-\Delta t/\tau} - \frac{\tau^2}{\Delta t} (1 - e^{-\Delta t/\tau}).$$

3.7. The UGKS relaxation part

A Crank-Nicolson based approximation is used for the relaxation part [22]. The numerical scheme is therefore:

$$F_{i,k}^{n+1}(\epsilon, \mathbf{i}) = F_{i,k}^{n}(\epsilon, \mathbf{i}) - \frac{\Delta t}{\Delta x} \left[\phi_{i+\frac{1}{2},k}^{n} - \phi_{i-\frac{1}{2},k}^{n} \right] (\epsilon, \mathbf{i}) + \frac{\Delta t}{2} \left[\left(\frac{G - F}{\tau} \right)_{i,k}^{n} + \left(\frac{G - F}{\tau} \right)_{i,k}^{n+1} \right] (\epsilon, \mathbf{i})$$
(47)

Classically, the equilibrium state at time t^{n+1} is computed based on the moments of F [11, 22], which are obtained from the moments of the microscopic scheme (47). This accurate technique could lead to a non-symmetric positive-definite tensor Θ and could compromise the calculation of a realistic equilibrium G^{n+1} . This is why we use instead a backward Euler relaxation term for the macroscopic scheme:

$$\boldsymbol{W}_{i}^{n+1} = \boldsymbol{W}_{i}^{n} - \frac{\Delta t}{\Delta x} \left[\boldsymbol{\Phi}_{i+\frac{1}{2}}^{n} - \boldsymbol{\Phi}_{i-\frac{1}{2}}^{n} \right] + \Delta t \left(\frac{\boldsymbol{V} - \boldsymbol{W}}{\tau} \right)_{i}^{n+1}, \tag{48}$$

where Φ and V are defined as follows:

$$\mathbf{\Phi} = \langle \mathbf{m}\phi \rangle_{\mathcal{V},\epsilon,i}, \quad \mathbf{V} = \langle \mathbf{m}G \rangle_{\mathcal{V},\epsilon,i}. \tag{49}$$

4. Numerical results

To assess the effectiveness of incorporating the collision process into the characteristic method (33) used to define numerical fluxes, we introduce the KO2 scheme, which is formulated without these relaxation effects. Thus, this scheme recovers the same behavior as UGKS only in the free molecular regime. We also compare our results with PIClas [18], a stochastic code that also solves the Pfeiffer ES-BGK model [13, 17].

4.1. The Couette flow

In the Couette configuration, the gas flows between two parallel, isothermal, infinite plates. One plate is stationary, while the other moves with a finite velocity u_w in the tangential y-direction. Under the continuum approximation, with no slip boundary conditions, the compressible Navier-Stokes-Fourier equations (CNS) yield to:

$$u_y(x) = \frac{x}{L}u_w, \quad T(x) = T_w + \frac{1}{2}\frac{\Pr x(L-x)}{c_p}u_w^2.$$
 (50)

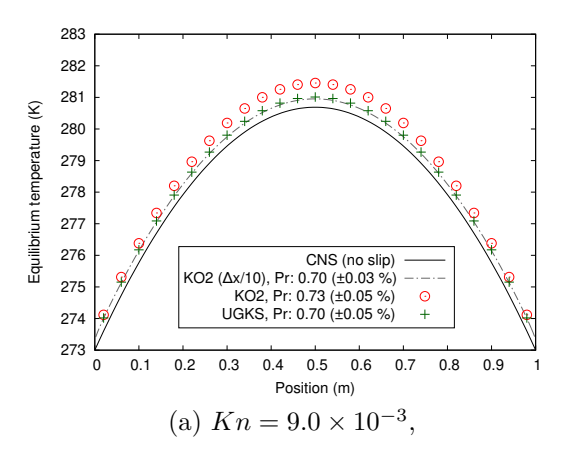
The Knudsen number of the flow is here defined as: $Kn = \mu_{ref}/(L\rho\sqrt{R_sT_w})$. Simulations are conducted in a near-continuum regime, at different Knudsen numbers by varying the initial mass density of the flow.

The parameters defining the gas are taken constant as follows: the specific constant R_s is 296.8 J kg⁻¹ K⁻¹, the viscosity μ is 1.656×10^{-5} Po, the Prandtl number Pr is 0.71, the degree of freedom number δ is 2.0, the average number $Z_{\rm rot}$ is set to 5.0, and the ES-BGK model of Andriès [1] is used since the vibrational mode of energy is not excited. Furthermore, the boundary walls are separated by a distance $L=1\,\rm m$, are maintained at 273 K and the velocity $u_{\rm w}$ is set to 300 m s⁻¹.

The spatial domain is discretized exclusively in the x-direction using 25 uniform cells. The velocity grid is Cartesian, defined over the range $[\pm 1200] \times [-1200, +1500] \,\mathrm{m\,s^{-1}}$, with 50 velocity points in both the x- and y-directions.

Figure 1 presents comparisons of the UGKS and KO2 schemes with the CNS solutions at different Knudsen numbers. Simulations with the KO2 scheme and a finer mesh have been conducted to highlight the deviation of the CNS solution from the rarefied flow solutions caused by the boundary conditions.

First, Figure 1 demonstrates the ability of both UGKS and KO2 schemes to resolve near-continuum flows. However, the UGKS achieves better accuracy on the same mesh. More precisely, as the Knudsen number decreases, the KO2 predictions increasingly deviate, while the UGKS predictions remain stable. Second, using the temperature equation (50), the Prandtl number can be roughly evaluated through a parabolic regression using the least squares method. The estimations on Figure 1 show the excellent capability of UGKS to simulate a correct Prandtl number for a given mesh, compared to the KO2 scheme.



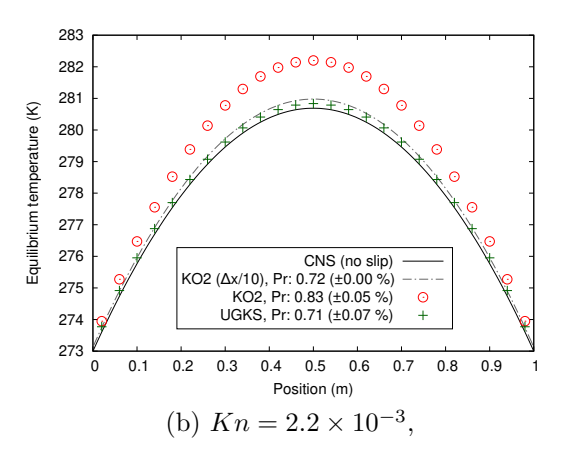
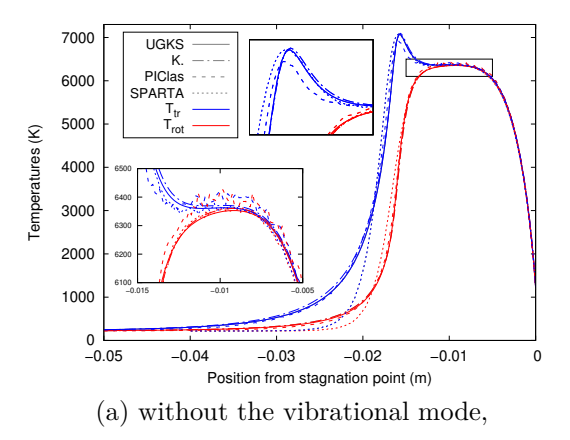


Fig 1. Comparison of UGKS and KO2 schemes with CNS solution in 1D Couette flow, and their Prandtl estimations using regressions (Given Pr. 0.71, $Z_{rot} = 5.0$).



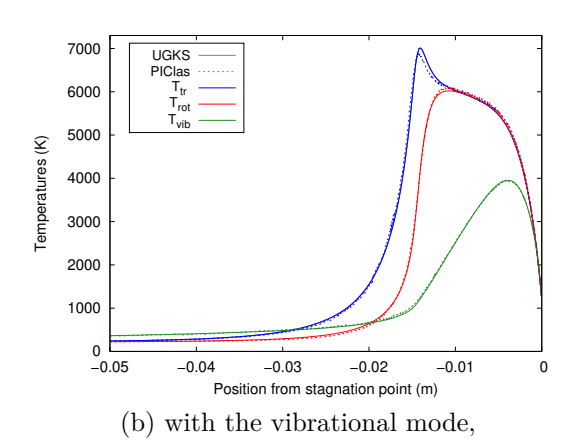


Fig 2. Comparison temperatures profiles on the stagnation line of a cylinder in a hypersonic flow, without consideration of vibrational energy.

4.2. Hypersonic flow passing a infinite cylinder

The 2D flow studied here is a hypersonic flow of dinitrogen around an infinite cylinder, representative of the conditions at an altitude of 70 km [5]. Given the hypersonic and rarefied nature of the flow, a smooth shock forms in front of the cylinder, and non-equilibrium effects occurring within it are particularly noticeable. Additionally, the conversion of a major part of kinetic energy into thermal energy behind the shock results in a sufficient increase in temperature to excite the vibrational mode of the particles. Consequently, the ES-BGK model chosen to model these non-equilibrium phenomena is that of Pfeiffer et al. [13].

The gas parameters are mostly identical to those used in the previous case, except for the viscosity, the Prandtl number, and the vibrational relaxation parameters. The viscosity is computed according to the VSS model with viscosity reference $\mu_{ref} = 1.656 \times 10^{-5} \,\mathrm{Po}$ at $T_{ref} = 273.15 \,K$, viscosity index $\omega = 0.74$ and scattering parameter $\alpha = 1.36$. The Prandtl is determined according to the Eucken formula, the collision number Z_{vib} is set as a constant to 200, and the characteristic temperature of vibration is $T_0 = 3371 \,K$. The spatial domain is again reduced to 2D using a reduced distribution technique and meshed around a cylinder with a radius of 4 cm maintained at temperature $T_w = 1000 \,K$. The velocity grid is also 2D bounded and discretized in both the x and y-direction.

First, a simulation excluding the vibrational energy mode is set up to compare our adaptation of UGKS with other approaches of the literature. Consequently, we conducted computation with the open-source DSMC code SPARTA [19], the stochastic ES-BGK solver PIClas [9, 18], and the deterministic finite volume ES-BGK solver developed at CEA, referred to as K. [2]. Comparisons are performed along the stagnation line and are presented in Figure 2(a). Good agreement can be observed between those codes. The primary difference is the shock expansion predicted by ES-BGK based codes compared to SPARTA which emulates the Boltzmann equation. This well-known behavior of BGK and ES-BGK models is generally attributed to the independence of the relaxation time τ on higher moments of the microscopic distribution, the distribution itself [4] or particle velocities [14]. Another difference appears in the peak translational temperature: while UGKS, K., and SPARTA yield similar values (within 0.15%), PIClas slightly underpredicts this maximum, with a deviation of -2.12% compared to UGKS.

Second, the vibrational mode is included. Since the energy relaxation mechanisms used in SPARTA and K. are not easily compatible with the relaxation law prescribed by the ES-BGK model of Pfeiffer, comparisons are restricted here to PIClas and UGKS only and are presented in Figure 2(b). As before, an excellent agreement in the modal temperature profiles can be observed as well as a restricted difference in the translational temperature peak value (-1.71%).

5. Conclusion

We proposed an extension of the Unified Gas-Kinetic Scheme (UGKS) to ES-BGK models that incorporates specific diatomic modes of energy. This adaptation extends the UGKS-ES-BGK framework from monoatomic to diatomic gases using techniques similar to those applied in extending UGKS-BGK to Shakhov and Rykov models. The method shows good agreements both for a near-continuum 1D viscous-driven flow and a rarefied 2D hypersonic flow, under both under-resolved and well-resolved mesh conditions.

References

- [1] P. Andriès, P. Le Tallec, J.-P. Perlat et B. Perthame: The Gaussian-BGK Model of Boltzmann Equation with Small Prandtl Number. Research Report RR-3716, INRIA, 1999. Projet M3N.
- [2] C. Baranger, J. Claudel, N. Hérouard et L. Mieussens: Locally refined discrete velocity grids for stationary rarefied flow simulations. *Journal of Computational Physics*, 257:572–593, 2014.
- [3] P. L. Bhatnagar, E. P. Gross et M. Krook: A model for collision processes in gases. i. small amplitude processes in charged and neutral one-component systems. *Phys. Rev.*, 94:511–525, 5 1954.
- [4] G. A. BIRD: Molecular Gas Dynamics and the Direct Simulation of Gas Flows. Oxford Science Publications, 1994.
- [5] I.D. BOYD et T. E. SCHWARTZENTRUBER: Models for Nonequilibrium Thermochemistry, page 252–310. Cambridge Aerospace Series. Cambridge University Press, 2017.
- [6] S. Chen, K. Xu et Q. Cai: A comparison and unification of ellipsoidal statistical and shakhov bgk models. Advances in Applied Mathematics and Mechanics, 7(2):245–266, 2015.
- [7] Songze Chen et Kun Xu: A comparative study of an asymptotic preserving scheme and unified gas-kinetic scheme in continuum flow limit. *Journal of Computational Physics*, 288:52–65, 2015.

- [8] Y. Dauvois, J. Mathiaud et L. Mieussens: An es-bgk model for polyatomic gases in rotational and vibrational nonequilibrium. *European Journal of Mechanics B/Fluids*, 88:1–16, 2021.
- [9] S. FASOULAS, C.-D. MUNZ, M. PFEIFFER, J. BEYER, T. BINDER, S. COPPLESTONE, A. MIRZA, P. NIZENKOV, P. ORTWEIN et W. RESCHKE: Combining particle-in-cell and direct simulation monte carlo for the simulation of reactive plasma flows. *Physics of Fluids*, 31(7):072006, 07 2019.
- [10] L. H. HOLWAY: Kinetic theory of shock structure using an ellipsoidal distribution function. *Rarefied Gas Dynamics, Volume 1*, 1:193–215, 1965.
- [11] S. LIU et C. ZHONG: Investigation of the kinetic model equations. Phys. Rev. E, 89:033306, 3 2014.
- [12] J. A. LORDI et R. E. MATES: Rotational Relaxation in Nonpolar Diatomic Gases. *The Physics of Fluids*, 13(2):291–308, 02 1970.
- [13] J. Mathiaud, L. Mieussens et M. Pfeiffer: An es-bgk model for diatomic gases with correct relaxation rates for internal energies. *European Journal of Mechanics B/Fluids*, 96:65–77, 2022.
- [14] L. MIEUSSENS et H. STRUCHTRUP: Numerical comparison of Bhatnagar–Gross–Krook models with proper Prandtl number. *Physics of Fluids*, 16(8):2797–2813, 08 2004.
- [15] R. C. MILLIKAN et D. R. WHITE: Systematics of Vibrational Relaxation. *The Journal of Chemical Physics*, 39(12):3209–3213, 12 1963.
- [16] J. G. Parker: Rotational and Vibrational Relaxation in Diatomic Gases. *The Physics of Fluids*, 2(4):449–462, 07 1959.
- [17] M. PFEIFFER: Extending the particle ellipsoidal statistical bhatnagar-gross-krook method to diatomic molecules including quantized vibrational energies. *Physics of Fluids*, 30(11):116103, 11 2018.
- [18] M. PFEIFFER: Particle-based fluid dynamics: Comparison of different bhatnagar-gross-krook models and the direct simulation monte carlo method for hypersonic flows. *Physics of Fluids*, 30(10):106106, 10 2018.
- [19] S. J. PLIMPTON, S. G. MOORE, A. BORNER, A. K. STAGG, T. P. KOEHLER, J. R. TORCZYNSKI et M. A. Gallis: Direct simulation monte carlo on petaflop supercomputers and beyond. *Physics of Fluids*, 31(8):086101, 08 2019.
- [20] E. M. Shakhov: Generalization of the krook kinetic relaxation equation. Fluid Dynamics, 3(5):95 96, 1968.
- [21] P. WELANDER: On the temperature jump in a rarefied gas. Ark. Fys., 7:507–553, 1954.
- [22] K. Xu et J.-C. Huang: A unified gas-kinetic scheme for continuum and rarefied flows. *Journal of Computational Physics*, 229(20):7747–7764, 2010.
- [23] K. Xu et J.-C. Huang: An improved unified gas-kinetic scheme and the study of shock structures. *IMA Journal of Applied Mathematics*, 76(5):698–711, 03 2011.